CHARACTERIZATION OF THE RELATIONSHIP BETWEEN BICUSPID AORTIC VALVE MORPHOLOGY AND HEMODYNAMICS

A Thesis
Presented to
The Academic Faculty

by

Daniel J. Mangiameli

In Partial Fulfillment
of the Requirements for the Degree
B.S. in Biomedical Engineering with Research Option in the
School of Wallace H. Coulter Department of Biomedical Engineering

Georgia Institute of Technology
December 2015

CHARACTERIZATION OF THE RELATIONSHIP BETWEEN BICUSPID AORTIC VALVE MORPHOLOGY AND HEMODYNAMICS

Approved by:

Dr. Ajit P.Yoganathan, Advisor
School of Biomedical Engineering
Georgia Institute of Technology

Dr. Wei Sun
School of Biomedical Engineering
Georgia Institute of Technology

Date Approved: December 7th, 2015

ACKNOWLEDGEMENTS

I would hereby like to acknowledge the members of the Cardiovascular Fluid Mechanics Laboratory at the Georgia Institute of Technology for their frequent advice on both the study and manuscript. I want to thank Dr. Ajit Yoganathan for giving me this amazing opportunity to work in the CFM lab. I also want to thank Dr. Neelakantan Saikrishnan for his early mentorship in the lab and Dr. Lucia Mirabella for all her support and guidance with the protocol. In addition, I would like to thank Dr. Alex Barker and Dr. Michael Markl from Northwestern University for their continued collaboration. Finally I would like to thank Dr. Vrishank Raghav for his support throughout the further refinement of the protocol and continued advice on this manuscript. The study was funded in part by NHLBI grant R01HL115828, American Heart Association Scientist Development grant 13SDG14360004 and K25HL119608, and the Wallace H. Coulter Distinguished Faculty Chair endowment.

TABLE OF CONTENTS

LIST OF TABLES

LIST OF FIGURES

NOMENCLATURE

BAV	Bicuspid Aortic Valve
MRI	Magnetic Resonance Imaging
bSSFP	Balanced Steady-state Free Precession
TAV	Tricuspid Aortic Valve
RN	Right-Non Coronary
RL	Right-Left Coronary
LN	Left-Non Coronary
AoSA	Aortoseptal Angle
AVR	Aortic Valve Replacement
VMTK	Vascular Modeling Toolkit
AAo	Ascending Aorta
WSS	Wall Shear Stress

ABSTRACT

Bicuspid aortic valve (BAV) is the most common congenital heart defect and may lead to secondary aortopathy such as aortic valve stenosis and regurgitation, potentially causing noticeable symptoms such as shortness of breath, chest pain, and dizziness. Although previously overshadowed by the genetic theory, there has recently been a belief that hemodynamics may play a larger role in the cause of secondary aortopathy in BAV than previously thought. However, hemodynamic studies have been impeded by lengthy data analysis protocols limiting their effectiveness and reproducibility. This work applied and further refined a novel semi-automated technique developed during a pilot study to process and analyze MRI data of the aorta and aortic valve based on 2D bSSFP cine and 4D flow MRI. The results were then used to characterize the morphology and hemodynamics between BAV fusion patterns. The protocol was applied to 24 size-matched TAV controls (n =24, mid ascending aorta (MAA) diameter =38.0$\pm$4.9 mm) and 28 BAV patients with aortic dilatation (n =14 RL-BAV, MAA diameter =38.1$\pm$5.3 mm; n =14 RN-BAV, 36.5$\pm$6.6 mm). RN-BAV subjects displayed a stronger correlation between hemodynamic metrics in the proximal AAo with diameter in the distal AAo when compared to size-matched TAV controls and RL-BAV subjects. The distal AAo diameter was found to be strongly correlated to the flow displacement ($R^2_{adjusted}$ =0.75) and flow angle ($R^2_{adjusted}$ =0.66) at the proximal AAo. Orifice circularity was also strongly correlated ($R^2_{adjusted}$ =0.53) to the distal AAo diameter in RN-BAV subjects. This study not only demonstrated the feasibility of a less user dependent protocol, but also highlighted several key metrics that are significantly different between fusion patterns of RN-BAV and RL-BAV patients.

CHAPTER 1

INTRODUCTION

Background

Bicuspid aortic valve (BAV) is the most common congenital heart defect and affects approximately 1-2% of the population (1). BAV patients exhibit bileaflet morphology as compared to a healthy trileaflet valve. This bileaflet morphology occurs during early fetal development due to the fusion of any two of the three leaflets (2). Although the most common type of fusion is between the right and left (RL) coronary leaflets, it may also occur between the right coronary and non-coronary (RN) or left coronary and non-coronary (LN) leaflets (1). BAV may progressively increase the likelihood of secondary pathologies such as aortic stenosis, valvular calcification, regurgitation, and aortic root dilatation (3,4). Symptoms include shortness of breath, chest pain, and dizziness. These secondary pathologies may lead to serious complications such as aortic aneurysm and heart failure. For reasons not well understood, not all BAV patients develop these conditions or exhibit the aforementioned symptoms (2).

There are two main theories concerning the development of secondary aortopathy in BAV patients. One school of thought claims it stems from genetics, whereas the other proposes the aortopathy is caused by a change in hemodynamics due to the valve morphology (5-7). Traditionally, the genetic theory has been more popular due to a larger number of studies investigating its influence. Nonetheless, a reevaluation of the current knowledge and practices regarding BAV proposes a greater acknowledgement of the hemodynamic effects (6). In light of this, recent studies have further analyzed geometric and hemodynamic biomarkers to better understand the progression of BAV (8-10). For example, one study used 4D MRI to demonstrate how the wall shear stress in the ascending aorta is significantly higher in BAV patients as

compared to that in TAV patients (11). Other researchers have investigated the aortoseptal angle (AoSA), which may be a significant factor in the hemodynamics of the aortic valve. The AoSA was reported as being significantly steeper in patients with isolated subaortic stenosis (12).

The aforementioned studies suggest hemodynamics may indeed play an important role in secondary aortic pathology and therefore must not be overlooked. Although the number of studies pertaining to hemodynamics has continued to increase, these investigations have been impeded by lengthy protocols needed to analyze different geometric and hemodynamic metrics, which greatly hinder integration into medical practice. A concise yet reliable method is needed in order for 4D MRI to become a standard in evaluating BAV related aortopathy.

In addition, recent studies have demonstrated a correlation between hemodynamic metrics dependent on leaflet fusion patterns such as wall shear stress, flow displacement, flow angle, and the phenotype of aortopathy in BAV subjects (7,8,11,13,14). However, most of these studies evaluated hemodynamic metrics in the vicinity of abnormal aortopathy in order to develop an understanding of the link between hemodynamics and the phenotype of BAV aortopathy. Associations between valvular structure and downstream hemodynamic metrics at independent sections have not been investigated; for example the influence of structure of the valve (e.g. fusion phenotype, valve opening area, eccentricity) on hemodynamic metrics in the proximal AAo and their relationship to markers of aortopathy. The development of such relationships could help further improve prognostic hemodynamic metrics for BAV subjects using standard of care imaging protocols (15) - for example a dynamic cine or phase-contrast MRI at the level of the aortic valve and/or sino-tubular junction which could provide prognostic morphologic or hemodynamic information. The motivation of this work aims to minimize imaging diagnostics and aid in prescription of preemptive patient specific surveillance and

therapeutic strategies. Thus, the aim of this study is to comprehensively characterize the impact of the upstream valve geometry, valve morphology (fusion pattern), or hemodynamics on the AAo geometry and hemodynamics at downstream aortic locations using 4D flow MRI data.

Literature Review

The mechanism of secondary aortopathy development from BAV disease is not well understood. There are two main theories; one claims it stems from genetics, whereas the other proposes the aortopathy rises from a change in hemodynamics due to valve morphology. The genetic theory has been more popular due to a higher number of studies investigating genetic influence. It is vital to know which theory is a better representation of the disease as the cause determines the surgical approach during treatment. For example, the popularity of the genetic theory and how BAV is a result of an irregularity of the vascular connective tissue has prompted more vigorous treatment plans for the proximal aorta (6).

Genetic theory would suggest that dilation of the aorta would often occur after aortic valve replacement (AVR) surgery, as is common with other connective tissue disorders. However, results of several studies show a large variability of about 5-30% between 10-20 years post AVR surgery. A possible link between aortic aneurysms and first-degree relatives has also been suggested (6). Furthermore, one study noted that patients with BAV had two or more family members that also presented BAV. Through the use of echocardiography, Huntington determined that 9.1% of first-degree relatives had BAV (16). Another important reasoning for the genetic theory is the prevalence of cystic medial degeneration in the wall of the ascending aorta, a type of degeneration also very common in Marfan syndrome patients (6).

One of the most common secondary pathologies from BAV is aortic dilatation. This dilation of the aorta can cause significant problems such as dissection, which may be fatal. The cause of

most aneurysms in the ascending aorta is unknown, unlike in the descending aorta where atherosclerosis is a common cause. A decrease in fibrillin-1 has been shown in BAV patients as compared to TAV patients. In addition, a mutation in the NOTCH1 gene leads to an alteration in signaling, which may be the cause of the formation of BAV and calcium accumulation on the valve. The varying expression of matrix metalloproteinase (MMPs) and Tissue inhibitors of metalloproteinase (TIMP) in BAV, TAV, and Marfan syndrome patients suggests that different mechanisms cause the aneurysms. Hemodynamics also is a factor because shear stress on the ascending aorta increases in BAV patients and the aortic diameter of BAV patients may be significantly larger even without stenosis or regurgitation, further demonstrating the complexity of BAV and the uncertainty about the progression of secondary pathologies (17).

Since several aortic pathologies generally associated with genetic factors are present even when genetics would not make a significant impact, support for the hemodynamic theory has grown. For example, cystic medial degeneration of the aorta wall has been frequently found in BAV patients and used as support for the genetic theory. However, studies have shown that the degeneration may occur even when genetics is not a factor, and therefore is a nonspecific characteristic. Furthermore, the tissue remodeling in BAV patients has been shown to be asymmetrical unlike in patients with Marfan syndrome. This asymmetry is believed to be a result of wall stress, an important aspect of the hemodynamic theory (6).

Considering the increased importance of the hemodynamic theory, Martijn den Reijer et al. (18) tested and demonstrated the relationship between irregular blood flow patterns in the ascending aorta and aortic dilatation. Quantifying this relationship is important because patients with “dilated aortas have a 9-fold increased risk of aortic dissection,” but sometimes BAV

patients exhibit no dilatation (18). It was demonstrated that an increased angle leads to an increase in dilation (18).

4D MRI is the combination of 3-dimensional imaging that is time-resolved and uses phase contrast. The use of 4D imaging has only recently been recognized as a practical way of studying cardiovascular diseases. Unusual blood flow is believed as a potential explanation for the varying progression of the disease based on the type of leaflet fusion. Additionally, the aforementioned study by Martijn den Reijer et al. (18) used several metrics pertaining to BAV patients that can be obtained from MRI data. Its lengthy protocol makes it clear that a concise yet reliable method is needed for 4D MRI to become a standard in evaluating BAV related aortopathy (18). In addition, another study used 4D cardiac MRI to characterize the relationship between blood flow and the development of ascending aortic dilation (11). The study sought to demonstrate how 4D flow could be used to study how blood flow affects the pathology of BAV patients. There was a long protocol for the analysis of the data, which included correcting the data before visualization, importing into 3D visualization software, and segmenting the wall. It was shown that wall shear stress significantly increased in BAV patients as compared to TAV patients. This study served as a building block for current research. Michael Hope et al. demonstrate a professional and effective way to conduct a pilot study and provide significant insight into a methodology of analyzing 4D flow data (11). The motivation of this work is to minimize complex imaging protocols to aid the ability to perform preemptive patient specific surveillance and therapeutic strategies. In order to achieve this goal, the aim here is to use a location commonly imaged as a part of standard of care to understand the impact of the upstream valve geometry, valve morphology (fusion pattern), or hemodynamics on the downstream AAo geometry and hemodynamics using 4D flow MRI data.

CHAPTER 2

MATERIALS AND METHODS

Subject Enrollment

A database of 151 subjects who received a cardiac MRI at Northwestern University between December 2011 and November 2012 was used to create two groups (BAV and TAV) of subjects for the study. Aortic stenosis or insufficiency determined to be greater than moderate was used as an exclusionary criterion. BAV and TAV cases were age-matched and composed of 28 BAV and 24 TAV cases. The BAV group was then subdivided into two groups based on leaflet fusion (14 RN and 14 RL). Due to the high prevalence of RL and RN fusion patterns (RL ≈ 80%, RN ≈ 17%) (7), the LN fusion pattern was not studied. The TAV cohort exhibited normal tricuspid valve function and did not have any history of cardiovascular disease. The Institutional Review Board of Northwestern University approved of this study, and authorized the release of their anonymized patient data, per the data sharing agreement with the Georgia Institute of Technology.

Magnetic Resonance Imaging

All subjects underwent cardiac MRI at 1.5T or 3T (Magnetom Espree, Avanto, Skyra or Trio Siemens Medical Systems, Germany). Cardiac MRI included ECG-gated, two-dimensional breathheld balanced steady-state free precessing (bSSFP) cine imaging to assess BAV morphology. In addition, 3D phase-contrast MRI, with three-directional velocity encoding (4D flow MRI) was acquired in a sagittal oblique volume covering the thoracic aorta. Prospective ECG gating was used with a respiratory navigator placed on the lung-liver interface (19). Pulse sequence parameters were as follows: flip angle of 15^{o}, spatial resolution of 1.7 - 3.7 mm by 1.8 -

2.6 mm by 2.2 - 3.7 mm, temporal resolution of 36.8 – 43.2 ms, total acquisition time, 8 to 15 minutes depending on heart rate and navigator efficiency, and velocity encoding range of 1 - 3 m/s (7).

Data Processing Protocol

Below are post-processing steps required to analyze the 2D bSSFP cine and 4D flow MRI data using a recently validated in-house semi-automated technique designed to extract aortic valve and aorta morphometry and hemodynamics (20).

Aortic Valve Region of Interest Determination

Due to multiple 2D cine data sets per case, the highest quality set was visually determined and imported into OsiriX® (v5.6; Pixmeo SARL, Bernex, Switzerland). The orifice and aortic root were then manually contoured at all cardiac time frames exhibiting an open aortic valve. This was performed using the closed polygon tool, which utilizes a spline interpolation based on user selected control points. In order to allow a precise measurement, the tool allows for continued readjustment of the control points. In addition, the closed polygon tool records both the area of the polygon and the coordinates of each control point. Peak systole was then determined as the frame with the largest orifice area. (Figure 1)

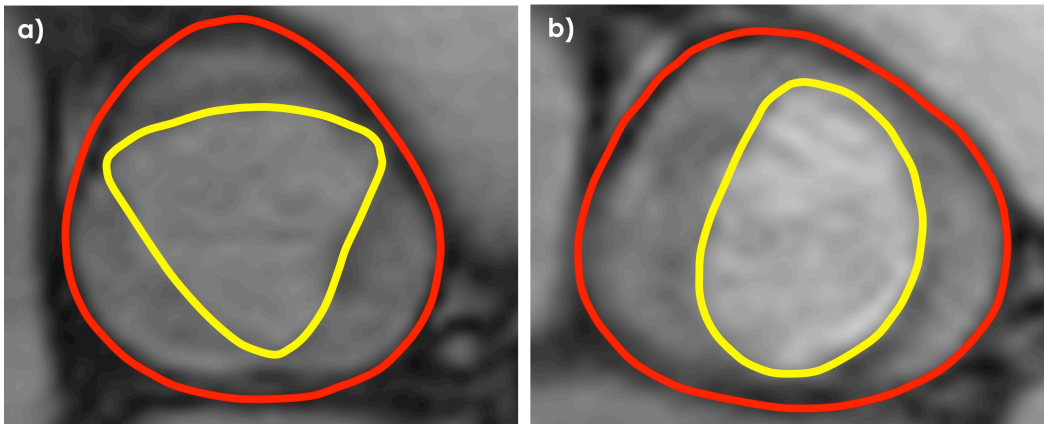

Figure 1. Example of orifice and aorta outline using the 2D cine MRI. a: TAV case; b: BAV case. In yellow: orifice outline; in red: aorta outline.

Anatomy and Velocity Segmentation of 4D Flow MRI Dataset

The 4D flow and magnitude data was then pre-processed with a custom MATLAB (Release 2012b, The MathWorks, Inc., Natick, Massachusetts, USA) program. This pre-processing step improved several common problems during data acquisition such as noise, velocity aliasing, and eddy currents (Figure 2). A video file of the processed data was then exported to allow for additional visualization of the corrections. To improve segmentation, the weighted sum over the resulting magnitude and phase contrast 3D stack of images were normalized by their maximum value. This 3D intensity field, which is at peak systole, was then processed and segmented using Vascular Modeling Toolkit (VMTK) software (http://www.vmtk.org), which aids in 3D reconstruction, geometric analysis, mesh generation and surface data analysis. The segmentation was performed between the aortic valve and the descending aorta on the same plane as to the aortic valve. Segmentation was achieved through user selected threshold values and seed points. The segmented vessel was then improved through scaling parameters in order to reduce sharp edges (Figure 3). The 3D image was converted into a 3D surface, smoothing was performed, and a volume mesh generated from the surface.

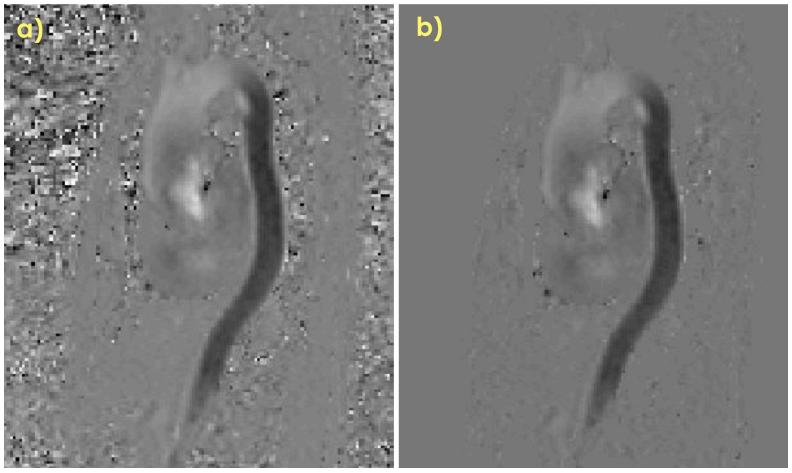

Figure 2. 4D flow and magnitude data pre-processing step. a: before pre-processing; b: after pre-processing.

Figure 3. Segmentation after the use of scaling parameters in VMTK.

Spatial Registration of 2D and 4D Data

The coordinates contained in the DICOM images and a rotation matrix were used to co-register the 2D data with the 3D data. In some cases, minor manual registration adjustments were needed where the breathheld 2D images were misaligned with the free-breathing 4D flow sequence. Paraview software (21) (v3.14, Clifton Park, NY, USA) was used to align the 2D and

the 3D MRI data, using a rigid translation to correct for any mismatch in the two datasets. To calculate the hemodynamic metrics, a reference system was created, as described in a previous paper by Mirabella et al. (20).

Processing and Analysis

The cine and 4D flow MRI data were then processed using an in-house robust and validated semi-automated technique (20). The need for lengthy manual data analysis, which limits reproducibility and/or integration into a clinically feasible workflow, is overcome using this semi-automated technique. The metrics derived from the MRI data included a) geometric – area of the valve orifice and aorta, circularity of the valve orifice and aorta, diameter of the aorta, and eccentricity of the valve orifice and b) hemodynamic – mean velocity, max velocity, flow angle, flow displacement, and jet quadrant. It was observed that one geometric and two hemodynamic metrics correlated well to distal ascending aortic diameter and are the primary discussion points in this work (Table 1; Figure 4). The other derived metrics are shown in Table 2. These metrics were evaluated at 11 equally spaced cross-sections ($S_{0\text{-}10}$) downstream of the valve annulus covering the ascending aorta and a part of the descending aorta as illustrated in Figure 4a. However, in this work we focus only on the ascending aorta up until the aortic arch ($S_{0\text{-}6}$).

Geometric metrics	
Orifice Circularity	$C_o = \frac{\int_\Omega dx}{\int_\Phi dx}$, where Ω is the region encompassing the orifice, and Φ is the smallest circle around Ω.
Hemodynamic metrics	

Flow angle	Angle between the mean velocity vector and a normal unit vector orthogonal to the analysis plane.
Flow displacement	Distance from the vessel centroid to the velocity-weighted centroid.

Table 1. Summary of data analysis metrics evaluated in this study. Please refer to Mirabella et al. (20) for detailed discussion on each of the metrics.

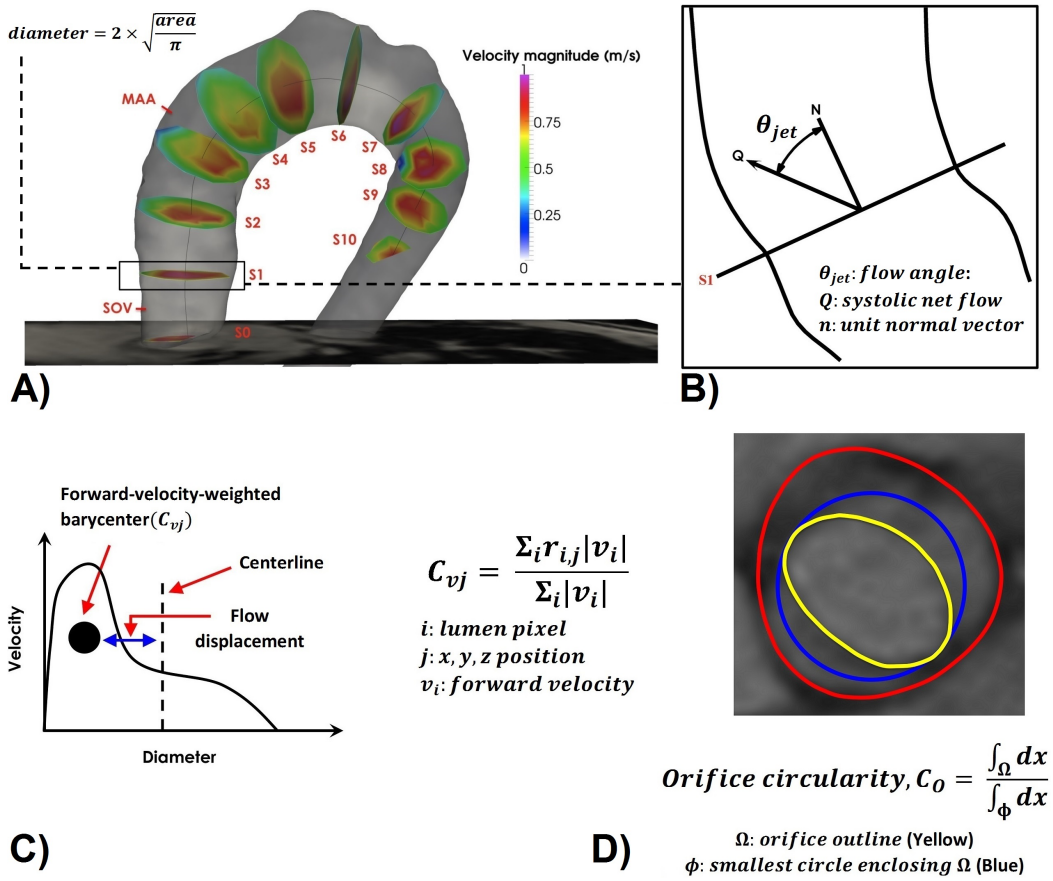

Figure 4. Illustration of different cross sections at which the analysis was performed. A: Reference system generated at the valve orifice and on the 10 cross-sections. B: Depiction of flow angle, ϕ jet. N, normal vector to the cross section; Q, mean velocity vector. C: Flow displacement. In blue: distance from the vessel barycenter to the velocity-weighted barycenter. D: Orifice circularity. Outline constructed during the aortic valve region of interest determination step.

Geometric metrics	
Area of the Valve Orifice and Aorta	Areas of the orifice and of the aorta's cross- section at the same location.
Diameter of the Aorta	$D_a = 2\sqrt{Area/\pi}$
Eccentricity	The distance between the barycenter of the orifice outline and the barycenter of the aorta outline on the same plane.
Hemodynamic metrics	
Mean Velocity	Magnitude of mean velocity vector on the cross-sectional plane
Maximum Velocity	Magnitude of maximum velocity vector on the cross-sectional plane
Jet Quadrant	The quadrant onto which the projection of the mean velocity vector on the cross-sectional plane lays.

Table 2. Summary of additional data analysis metrics evaluated in this study. Please refer to Mirabella et al. (20) for detailed discussion on each of the metrics.

Statistical Analysis

For each group, aorta size-matched TAV controls, RL-BAV, and RN-BAV a Shapiro-Wilk test was used to determine if the parameters were normally distributed. One-way ANOVA was used to compare hemodynamic and geometric parameters between the groups. Univariate and multivariate regression models were tested for each group to correlate geometric and hemodynamic metrics with distal AAo diameter. The quality of the data has been adjusted for the number of subjects in the analysis and hence the goodness of fit in the regression analysis is reported as $R^2_{adjusted}$, a conservative estimate when compared to R^2. Statistical analysis was performed using MATLAB (Release 2012b, The MathWorks Inc., Natick, Massachusetts, USA).

CHAPTER 3

RESULTS

Study Cohort

The protocol was applied to a cohort of 14 RN-BAV, 14 RL-BAV, and 24 TAV control subjects with the demographics summarized in Table 3. Size-matched TAV subjects were significantly ($p < 0.02$) older than patients with BAV. The mid ascending aorta diameter among all the groups were not significantly different. Aortic stenosis severity was mild (n = 0) and moderate (2) for TAV, mild (n = 2) and moderate (n = 1) for RL-BAV, and mild (n = 2) and moderate (n = 2) for RN-BAV subjects. Aortic insufficiency was present in (n = 7) of TAV, (n = 7) of RL-BAV, and (n = 9) of RN-BAV subjects. Eccentricity of the orifice was significantly larger in RN-BAV than TAV (2.0 ± 1.1 vs. 3.9 ± 1.6, $p < 0.02$). Normalized flow displacement at cross-section S_2 was significantly larger in both RL and RN-BAV subjects than size-matched TAV (0.17 ± 0.08 and 0.18 ± 0.10 vs. 0.11 ± 0.08, $p < 0.02$). Flow angle measured at cross-section S_2 was not significantly different among the three groups. A summary of the parameters computed along the aorta is shown in Figure 5.

		TAV	RL-BAV	RN-BAV
n (female)		24 (4)	14 (3)	14 (4)
Age		58.2 ± 13.3	47.2 ± 11.9 *	44.7 ± 8.3 *
Mid AAo diameter, mm		38.0 ± 4.9	38.1 ± 5.3	36.5 ± 6.6
Stenosis severity	Mild	0	2	2
	Moderate	2	1	2
	Severe	0	0	0
Aortic insufficiency	Mild	4	5	6
	Moderate	3	2	3
	Severe	0	0	0
Orifice eccentricity,		2.0 ± 1.1	2.0 ± 1.0	3.9 ± 1.6 *
Orifice circularity,		0.59 ± 0.10	0.62 ± 0.13	0.57 ± 0.14
Normalized flow displacement at S_2		0.11 ± 0.08	0.17 ± 0.08 *	0.18 ± 0.10 *
Flow angle at S_2 ^{o}		18.2 ± 10.5	23.5 ± 10.3	22.1 ± 17.9

Table 3. Summary of patient demographics, aortic dimensions, valve geometry and hemodynamic characteristics. All continuous data are presented as mean ± standard deviation. *Independent-sample t test indicates significant differences compared with size-matched controls ($p < 0.02$).

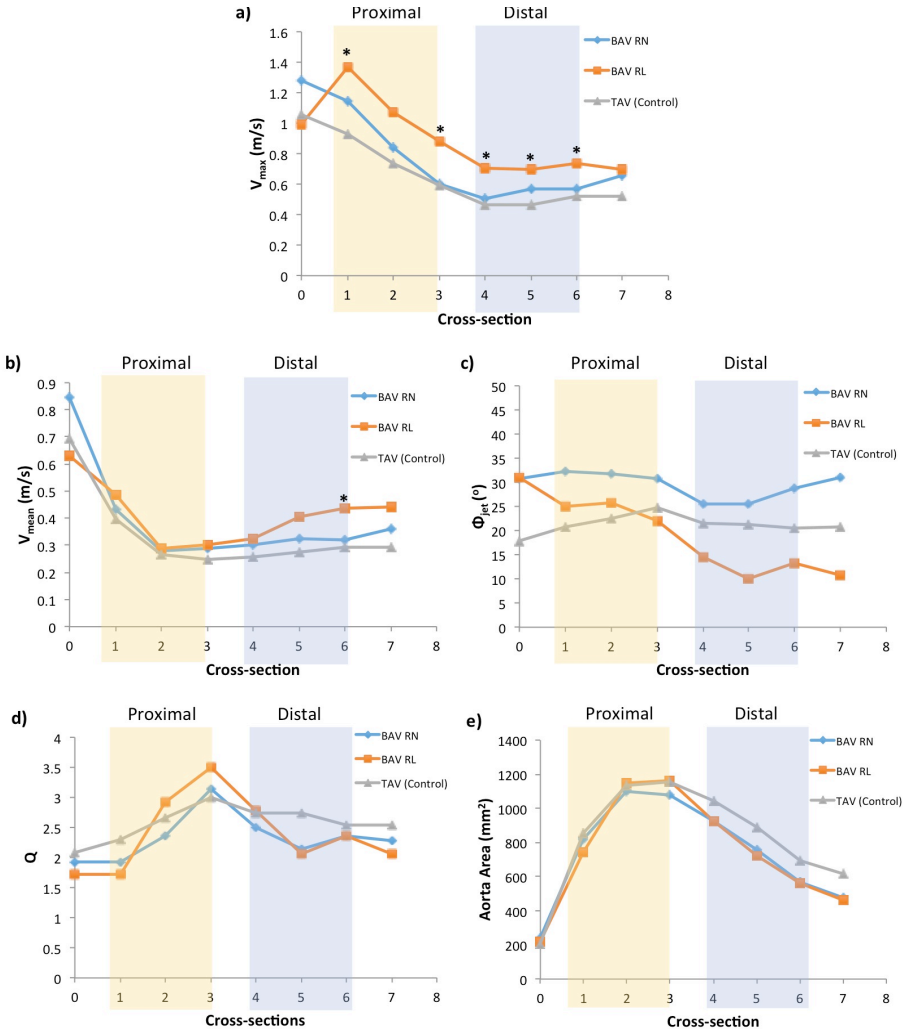

Figure 5. Mean values of the aorta and hemodynamic metrics along the aorta. Jet quadrant is express in terms of its median. The '*' indicates the section with a statistically significant difference between RL-BAV and TAV groups ($p < 0.05$). a: maximum velocity; b: mean velocity; c: jet angle; d: jet quadrant; e: area of aorta cross-sections.

Correlation between Hemodynamics and Ascending Aorta Diameter

It was observed that two hemodynamic metrics (flow displacement and flow angle) and one geometric metric (circularity of the valve orifice), summarized in Figure 6, correlated well to

distal AAo (S_4-S_6) diameter and are the primary discussion points in this work. As mentioned earlier, the hemodynamic metrics were evaluated at the approximate location of the sino-tubular junction (S_2). Our primary objective here was to develop an understanding of the relationship between hemodynamic metrics in the proximal ascending aorta and the diameter of the aorta in the distal portions. First, we investigated the impact of normalized flow displacement at section S_2 on aorta diameter at downstream sections $S_{3\text{-}6}$ for the three groups. Figure 6 illustrates the best regression results between normalized flow displacement at S_2 and aorta diameter at S_5 for the three groups. It was observed that all the groups had a positive association between normalized flow displacement at S_2 and aorta diameter at S_5. RN-BAV subjects had the highest correlation with a significant positive association ($R^2_{adjusted}$ = 0.75, slope = 54.8, $p < 0.01$), RL-BAV subjects had the weakest correlation ($R^2_{adjusted}$ = 0.01), and aorta size-matched TAV subjects had a moderately better correlation ($R^2_{adjusted}$ = 0.12, slope = 23.8, $p < 0.055$).

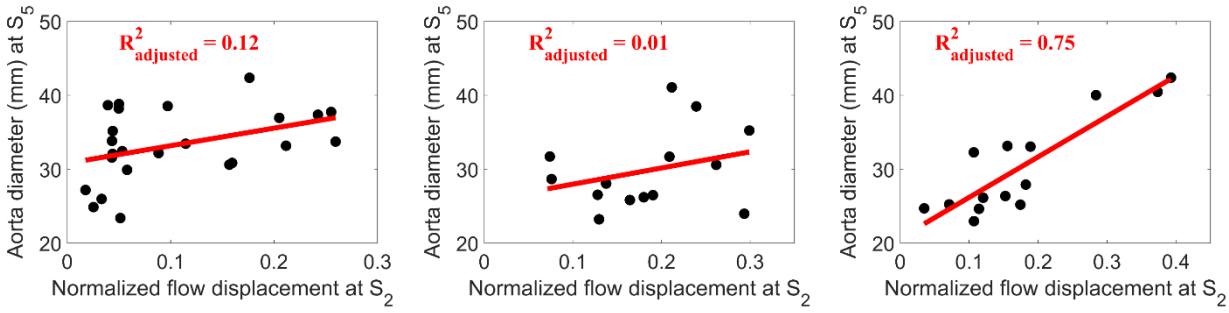

Figure 6. Scatter plot illustrating the correlation between normalized flow displacement at S_2 and aorta diameter at S_5. Left - TAV, center – RL-BAV, right – RN-BAV.

Table 4 summarizes the rest of the linear regression results for the correlation between normalized flow displacement at S_2 and downstream aortic diameter at $S_{3\text{-}6}$. RN-BAV subjects exhibited a positive association between normalized flow displacement and aortic diameter; an increase in normalized flow displacement at S_2 was observed to cause a significant increase ($p < 0.01$) in downstream aortic diameter at cross-sections $S_{3\text{-}6}$. Although the goodness of fit was

relatively lower for TAV subjects when compared to RN-BAV subjects, the data exhibited a significant positive association ($p < 0.055$). Normalized flow displacement was observed to have a negligible impact on the downstream aorta diameter for RL-BAV subjects. The most significant observation here is that the flow displacement at S_2 is strongly associated with the ascending aortic diameter at S_5 for RN-BAV subjects.

Cross-section	TAV		RL-BAV		RN-BAV	
	$R^2_{adjusted}$	Slope	$R^2_{adjusted}$	Slope	$R^2_{adjusted}$	Slope
S_2	0.00	10.2	0.00	18.7	0.18	33.5
S_3	**0.18**	**28.0 ***	0.15	34.1	**0.42**	**42.8** †
S_4	**0.18**	**24.4 ***	0.07	24.8	**0.62**	**50.3** †
S_5	**0.12**	**23.8 ***	0.01	21.9	**0.75**	**54.8** †
S_6	0.03	14.1	0.00	7.6	**0.70**	**37.7** †

Table 4. Summary of linear regression coefficients for the correlation between normalized flow displacement at S_2 and aortic diameter at downstream cross-sections. † $p < 0.01$, * $p < 0.055$

Furthermore, our investigation revealed that the flow angle for RN-BAV subjects at section S_2 had the highest correlation and a significant positive association ($R^2_{adjusted} = 0.66$, slope = 0.32, $p<0.01$) with the diameter of the ascending aorta at section S_4 (Figure 7). RL-BAV subjects exhibited a weak correlation ($R^2_{adjusted} = 0.16$, slope = 0.23, $p<0.1$), while TAV subjects had the weakest correlation ($R^2_{adjusted} = 0.04$).

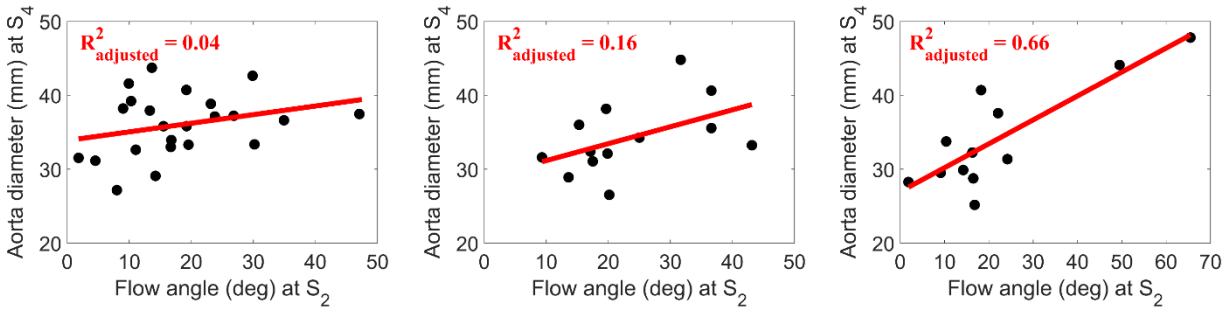

Figure 7. Scatter plot illustrating the correlation between flow angle at S_2 and aorta diameter at S_4. Left -TAV, center – RL-BAV, right – RN-BAV.

Table 5 summarizes the rest of the regression data between flow angle at S_2 and aortic diameter at downstream cross-sections. Flow angle at S_2 strongly correlated to most of the distal portions of the ascending aorta ($S_{3\text{-}5}$) for RN-BAV subjects, while the strongest correlation for RL-BAV subjects was observed at the immediately following cross-section (S_3). However, it should be noted that the significance of the positive association between flow angle and ascending aortic diameter was markedly different between the two groups, $p < 0.01$ vs. $p < 0.1$ for RN-BAV and RL-BAV subjects respectively.

Cross-section	TAV		RL-BAV		RN-BAV	
	$R^2_{adjusted}$	Slope	$R^2_{adjusted}$	Slope	$R^2_{adjusted}$	Slope
S_2	0.18	0.21	0.00	0.00	0.39	0.27
S_3	0.09	0.16 *	**0.21**	**0.26 ***	**0.53**	**0.30** †
S_4	0.04	0.11	**0.16**	**0.23 ***	**0.66**	**0.32** †
S_5	0.00	0.06	0.00	0.15	**0.49**	**0.29** †
S_6	0.00	0.03	0.00	0.05	0.34	0.18

Table 5. Summary of linear regression coefficients for the correlation between flow angle at S_2 and aortic diameter at downstream cross-sections. † $p < 0.01$, * $p < 0.1$.

Correlation between Valve Geometry and Ascending Aorta Diameter

Valve annular geometric parameters such as annulus circularity and eccentricity were evaluated for analysis and it was observed that annulus circularity best correlated with ascending aortic geometry. Figure 8 illustrates the best regression results between annulus circularity and ascending aorta diameter at S_2 for the three groups. It was observed that RN-BAV subjects had the highest correlation with a significant negative association ($R^2_{adjusted}$ = 0.53, slope = -36.9, $p < 0.01$), RL-BAV subjects had the weakest correlation ($R^2_{adjusted}$ = 0.00), and aorta size-matched TAV subjects had a moderate correlation with negative association ($R^2_{adjusted}$ = 0.26, slope = -26.5, $p < 0.06$).

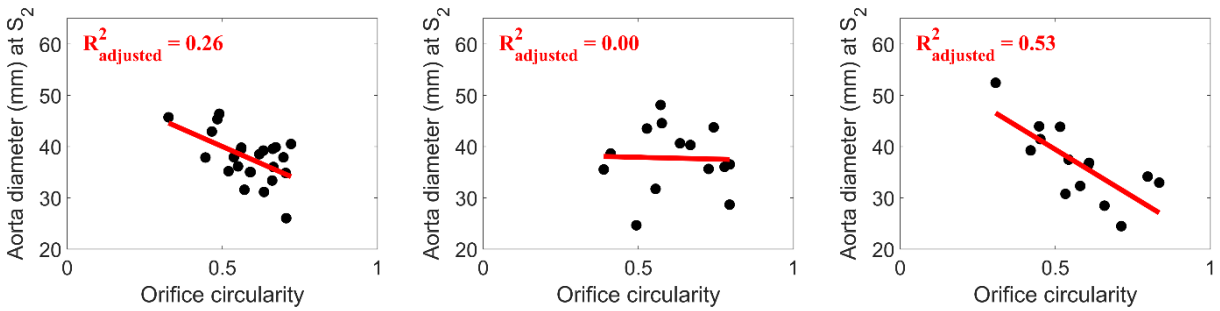

Figure 8. Scatter plot illustrating the correlation between orifice circularity and aorta diameter at S_2. Left - TAV, center – RL-BAV, right – RN-BAV.

Table 6 summarizes the linear regression results for the correlation between annulus circularity and downstream aortic diameter at $S_{2\text{-}6}$. RN-BAV subjects exhibited a negative association between annulus circularity and aortic diameter; a more circular annulus was observed to cause a significant decrease ($p < 0.01$) in downstream aortic diameter only at cross-sections $S_{2\text{-}4}$. Although the goodness of fit was relatively lower for TAV subjects when compared to RN-BAV subjects ($R^2_{adjusted}$ = 0.53 vs. 0.26), the data exhibited a significant negative association ($p < 0.06$). Furthermore, annulus circularity was observed to have no impact on the downstream aorta diameter for RL-BAV subjects. Across all the groups, annulus

circularity was strongly correlated only to the proximal portions of the ascending aorta and not to the distal portions of the ascending aorta.

Cross-section	TAV		RL-BAV		RN-BAV	
	$R^2_{adjusted}$	Slope	$R^2_{adjusted}$	Slope	$R^2_{adjusted}$	Slope
S_2	**0.26**	**-26.5 ***	0.00	-1.43	**0.53**	**-36.9 ***
S_3	**0.16**	**-22.1** †	0.00	-10.4	**0.28**	**-26.4** †
S_4	0.07	-14.4	0.07	-13.1	**0.20**	**-23.3** †
S_5	0.00	-2.0	0.01	-11.6	0.05	-15.8
S_6	0.00	3.1	0.06	-4.88	0.00	-0.6

Table 6. Summary of linear regression coefficients for the correlation between orifice circularity and aortic diameter at downstream cross-sections. † $p < 0.01$, * $p < 0.06$.

Multivariate Regression Analysis

Given the complex interdependency of geometry and flow, a multiple-regression analysis was performed in order to investigate the correlation between valve geometry and hemodynamics on the ascending aorta diameter. The two strongly correlated hemodynamic variables – flow angle and flow displacement and valve geometric variable – orifice circularity were used as the independent variables. The distal ascending aorta diameter (S_4) was used as the dependent variable in this multivariate regression analysis (Table 7 summarizes the results of this analysis). The strongest correlations in the multivariate analysis were observed in the RN-BAV subjects when compared with RL-BAV subjects and size-matched TAV controls ($R^2_{adjusted}$ = 0.79 vs 0.11 vs 0.18). Normalized flow displacement and flow angle were observed to have the most significant impact for RN-BAV subjects.

Subject cohort	Multiple Regression $R^2_{adjusted}$	Correlation coefficients (β)		
		Orifice Circularity	**Normalized Flow Displacement at S_2**	**Flow angle at S_2**
TAV	0.18	-11.45	22.61*	0.03
RL-BAV	0.11	-13.72	7.91	0.11
RN-BAV	0.79	-7.07	**28.43***	**0.18***

Table 7. Summary of linear multiple regression analysis of the strongly correlated ascending aorta hemodynamic and valve geometric variables with distal ascending aorta diameter (S_4). *$p<0.05$

CHAPTER 4

DISCUSSION

Protocol Development

An important part of the study was the continued refinement and application of a novel and semi-automatic protocol developed in a previous pilot study by Mirabella et al. (20) to characterize the relationship between bicuspid aortic valve morphology and hemodynamics. This protocol limits the amount of user dependent steps, reducing the time it takes for data analysis. Manual tasks that are possibly affected by user variability have been reduced to a minimum with only one fully manual step, which requires segmentation of the 2D contours of the valve. The 3D segmentation of the aortic lumen is semi-automatic, with the user selecting proper initialization and method parameters for the level-set algorithm. The user variability for the fully manual segmentation was assessed in a blind test by two readers using a Bland-Altman plot as described in a previous paper by Mirabella et al. (20). User variability was within the limits of agreement (± 1.96 SD), thus demonstrating an insignificant amount of variability. This study demonstrates the feasibility of the novel protocol by its application to a larger study. In addition, the robust capabilities of the protocol is shown in its ability to characterize differences in BAV fusion pattern and investigate the predictive potential of flow and geometry in the proximal AAo on the distal AAo diameter, which distinguishes its use as compared with the pilot study by Mirabella et al. (20).

Metrics Along the Aorta

One part of the study analyzed the change of different hemodynamic metrics along the aorta. As expected, the mean velocity profile tends to decrease in the proximal ascending aorta

and then increase in the distal ascending aorta. One reason is due to the size of the aorta, which is inversely proportional to the mean velocity. If cardiac output were constant in two differently sized aortas, the larger aorta would have a lower mean velocity. It was observed that RL-BAV subjects have a significantly higher maximum velocity than TAV patients for both the proximal and distal portions of the ascending aorta. This result is quite interesting because although the variation of area for the three cases is more or less the same, the maximum velocity changes quite significantly for RL-BAV. This is perhaps related to the flow angle and its effect on the max velocity. For the jet angle variation, although RL-BAV and RN-BAV fusion patterns both display a higher jet angle as compared to TAV in the proximal ascending aorta, they show opposite trends at the distal portions. This finding could suggest that the anatomy of the aorta, with 3D curvature and torsion, tends to smooth differences in flow eccentricity between the two groups as the flow progresses downstream towards the descending aorta. Although the mean values for RN-BAV and RL-BAV appear to be significant with regards to TAV, due to their high variability the results prove to be insignificant.

Effect of Valve Phenotype in the Proximal AAo to Distal AAo Diameter

This study utilized a validated semi-automated 4D flow MRI processing technique (20) to analyze a cohort of human subjects to correlate BAV valve phenotype related hemodynamics and geometry in the proximal AAo to the distal AAo diameter. Similar to previous findings (7,11,14), the presence of BAV and the type of cusp fusion pattern were accompanied by changes in systolic hemodynamic metrics as quantified by flow displacement and flow angle in the proximal AAo (S_2). The systolic hemodynamic metrics in the proximal AAo were strongly associated with the distal AAo diameter only in RN-BAV subjects, RL-BAV subjects exhibited a weak association, while size-matched TAV controls exhibited a moderate association. Flow

displacement and flow angle were not significantly different ($p = 0.77, 0.80$) between RL-BAV and RN-BAV subjects, which implies that the BAV phenotype related hemodynamics has a strong influence on the distal AAo aortopathy. These observations agree with prior work (7,14), where the systolic jet in RN-BAV subjects has been observed to "bounce" off the proximal AAo before impinging on the distal ascending aorta, which could be the primary cause for the observed correlation. These findings could imply that the distal AAo diameter in RN-BAV group is more susceptible to hemodynamic alterations in the proximal AAo, while the RL-BAV group is not affected by hemodynamics and likely more dependent on the genetics.

The valve geometric metric as quantified by orifice circularity was observed to be associated strongly with the distal AAo diameter only for the RN-BAV subjects. Similar to the hemodynamic metrics, the circularity of the orifice does not vary significantly between the subject cohorts, however, only RN subjects exhibit a strong correlation between valve orifice circularity and distal AAo diameter. Unlike hemodynamic metrics, valve orifice circularity was strongly correlated only to the diameter of the proximal portions of the AAo and not to the distal portions of the AAo.

The multivariate regression analysis did not reveal any significant correlations in RL-BAV or size-matched TAV control subjects, when compared to the RN-BAV subjects. Among the RN-BAV subjects, systolic hemodynamics (flow displacement and flow angle) in the proximal AAo plays a more critical role ($p < 0.05$) than the valve geometric metrics (orifice circularity). This finding suggests the systolic hemodynamic metrics in the proximal AAo are sufficient to be used as prognostic metrics for distal AAo remodeling.

Implications on BAV Diagnosis and Management

The findings of this work encourage the usage of standard of care imaging (for example PC-MRI, as demonstrated by recent reports (22) to measure changes in AAo hemodynamics) at the level of the sino-tubular junction, which could provide hemodynamic information informing the resulting downstream effects. Furthermore, based on recent results on prognostic significance of altered hemodynamics in BAV patients (15), the findings in this work suggest that the presence of flow abnormality in the proximal AAo could be used to risk-stratify BAV patients for the possibility of developing distal AAo aortopathy. This could help in fine-tuning risk assessment and aid in prescription of preemptive patient specific surveillance and therapeutic strategies.

Study Limitations

One limitation of this study is the need for manual 2D and 4D segmentation, which lengthens data processing and introduces user variability. However, most computed hemodynamic variables were based on the mean velocity vector, which is not highly sensitive to point-wise measurement errors. Longitudinal studies are critical to improve the current understanding of the relationship between BAV phenotype/morphology to aortopathy risk stratification. In order to connect the diagnostic suggestions in this work, the evaluation of better indicators of remodeling, for example wall shear stress (WSS), needs to be considered in the distal AAo and correlated to flow displacement and/or flow angle in the proximal AAo. Nonetheless, the measurement of WSS was not within the scope of this work.

CHAPTER 5

CONCLUSIONS

This study developed a novel semi-automatic protocol to analyze 2D cine and 4D flow MRI data acquisitions in order to study hemodynamics relating to BAV. This protocol was applied to a large cohort of BAV subjects to characterize the relationship between BAV morphology and hemodynamics. It was shown that the hemodynamics in the proximal AAo is significantly correlated to the distal AAo diameter in RN-BAV subjects when compared to RL-BAV and size-matched TAV controls. The measurements of upstream hemodynamic metrics play a more significant role than geometric metrics of the valve orifice when considering downstream aortic size.

CHAPTER 6

RECOMMENDATIONS

The combination of using geometrical and hemodynamic predictors for BAV disease can have an even greater clinical impact if, for example, this study could be further extended to include more complex flow metrics, which might be indicators of flow disturbances (e.g., vorticity, helicity, wall shear stress, oscillatory shear index), or it could take into account other metrics easily clinically categorized. In addition, longitudinal studies could be performed to improve the current understanding of the relationship between BAV phenotype/morphology to aortopathy risk stratification. The work presented here can be regarded as yet another step to find geometrical and hemodynamic predictors to assess the severity of the disease or its progression.

REFERENCES

1. Go A.S., Mozaffarian D, Roger V.L. et al. Heart disease and stroke statistics--2014 update: a report from the American Heart Association. Circulation 2014;129:e28-e292.
2. Svensson L. Bicuspid Aortic Valve Disease. 2014.
3. Mordi I, Tzemos N. Bicuspid aortic valve disease: a comprehensive review. Cardiol Res Pract 2012;2012:196037.
4. Ward C. Clinical significance of the bicuspid aortic valve. Heart 2000;83:81-85.
5. Barker AJ, Markl M. The role of hemodynamics in bicuspid aortic valve disease. European journal of cardio-thoracic surgery : official journal of the European Association for Cardio-thoracic Surgery 2011;39:805-6.
6. Girdauskas E, Borger MA, Secknus MA, Girdauskas G, Kuntze T. Is aortopathy in bicuspid aortic valve disease a congenital defect or a result of abnormal hemodynamics? A critical reappraisal of a one-sided argument. European journal of cardio-thoracic surgery : official journal of the European Association for Cardio-thoracic Surgery 2011;39:809-14.
7. Mahadevia R, Barker AJ, Schnell S et al. Bicuspid Aortic Cusp Fusion Morphology Alters Aortic Three-Dimensional Outflow Patterns, Wall Shear Stress, and Expression of Aortopathy. Circulation 2014;129:673-682.
8. Bissell MM, Hess AT, Biasiolli L et al. Aortic dilation in bicuspid aortic valve disease: flow pattern is a major contributor and differs with valve fusion type. Circulation Cardiovascular imaging 2013;6:499-507.
9. Hahn RT, Roman MJ, Mogtader AH, Devereux RB. Association of aortic dilation with regurgitant, stenotic and functionally normal bicuspid aortic valves. Journal of the American College of Cardiology 1992;19:283-8.
10. Meierhofer C, Schneider EP, Lyko C et al. Wall shear stress and flow patterns in the ascending aorta in patients with bicuspid aortic valves differ significantly from tricuspid aortic valves: a prospective study. European heart journal cardiovascular Imaging 2013;14:797-804.
11. Hope MD, Hope TA, Crook SE et al. 4D flow CMR in assessment of valve-related ascending aortic disease. JACC Cardiovascular imaging 2011;4:781-7.
12. Sigfusson G, Tacy TA, Vanauker MD, Cape EG. Abnormalities of the left ventricular outflow tract associated with discrete subaortic stenosis in children: an echocardiographic study. Journal of the American College of Cardiology 1997;30:255-9.
13. Hope MD, Hope TA, Meadows AK et al. Bicuspid Aortic Valve: Four-dimensional MR Evaluation of Ascending Aortic Systolic Flow Patterns. Radiology 2010;255:53-61.
14. Kang JW, Song HG, Yang DH et al. Association Between Bicuspid Aortic Valve Phenotype and Patterns of Valvular Dysfunction and Bicuspid Aortopathy Comprehensive Evaluation Using MDCT and Echocardiography. Jacc-Cardiovasc Imag 2013;6:150-161.
15. Burris NS, Sigovan M, Knauer HA, Tseng EE, Saloner D, Hope MD. Systolic Flow Displacement Correlates With Future Ascending Aortic Growth in Patients With Bicuspid Aortic Valves Undergoing Magnetic Resonance Surveillance. Invest Radiol 2014;49:635-639.

16. Huntington K, Hunter AG, Chan KL. A prospective study to assess the frequency of familial clustering of congenital bicuspid aortic valve. Journal of the American College of Cardiology 1997;30:1809-12.
17. Tadros TM, Klein MD, Shapira OM. Ascending aortic dilatation associated with bicuspid aortic valve: pathophysiology, molecular biology, and clinical implications. Circulation 2009;119:880-90.
18. den Reijer PM, Sallee D, 3rd, van der Velden P et al. Hemodynamic predictors of aortic dilatation in bicuspid aortic valve by velocity-encoded cardiovascular magnetic resonance. Journal of cardiovascular magnetic resonance : official journal of the Society for Cardiovascular Magnetic Resonance 2010;12:4.
19. Markl M, Harloff A, Bley TA et al. Time-resolved 3D MR velocity mapping at 3T: Improved navigator-gated assessment of vascular anatomy and blood flow. J Magn Reson Imaging 2007;25:824-831.
20. Mirabella L, Barker AJ, Saikrishnan N et al. MRI-based Protocol to Characterize the Relationship Between Bicuspid Aortic Valve Morphology and Hemodynamics. Ann Biomed Eng 2014;43:1815-1827.
21. Squillacote AH. The ParaView Guide: A Parallel Visualization Application.: Kitware Inc., 2008.
22. Burris NS, Hope MD. Bicuspid Valve-Related Aortic Disease: Flow Assessment with Conventional Phase-Contrast MRI. Acad Radiol 2015;22:690-696.